Highlights:

- Ribbons crystallize into a single-phase hexagonal Ni_2In-type at room temperature.
- A magnetic-field-induced AFM-FM transition of martensite structure was observed.
- The annealed ribbons showed a first-order magnetostructural transition (MST).
- Quasi-reversible character of magnetic entropy change was observed at MST.
- The annealed ribbons exhibit a large magnetocaloric effect at MST.

Large reversible magnetic entropy change in rapidly solidified $Ni_{0.895}Cr_{0.105}MnGe_{1.05}$ melt-spun ribbons

Anil Aryal[1, a], Abdiel Quetz[1], C.F. Sánchez-Valdés[2], P.J. Ibarra-Gaytán[3], Sudip Pandey[1], Igor Dubenko[1], J.L. Sánchez Llamazares[3, b], Shane Stadler[4], and Naushad Ali[1]

[1]Department of Physics, Southern Illinois University, Carbondale, IL 62901 USA

[2]División Multidisciplinaria, Ciudad Universitaria, Universidad Autónoma de Ciudad Juárez (UACJ), calle José de Jesús Macías Delgado # 18100, Ciudad Juárez, Chihuahua, México.

[3]Instituto Potosino de Investigación Científica y Tecnológica A.C., Camino a la Presa San José 2055, Col. Lomas 4ª, San Luis Potosí, S.L.P. 78216, México.

[4]Department of Physics & Astronomy, Louisiana State University, Baton Rouge, LA 70803 USA

ABSTRACT:

The crystal structure, and magnetic and magnetocaloric properties of rapidly solidified $Ni_{0.895}Cr_{0.105}MnGe_{1.05}$ melt-spun ribbons is reported. The ribbon samples crystallize into a single-phase hexagonal Ni_2In-type structure at room temperature. The as-quenched ribbons showed a second order magnetic transition at 192 ± 1 K at $\mu_o H$ = 5 mT. A magnetic-field-induced transition from an antiferromagnetic (AFM)-like to a ferromagnetic (FM) state of martensite structure was observed in annealed ribbons below the temperature of the martensitic transformation (T_M ~ 245 ± 1 K). The annealed ribbons undergo a first-order magnetostructural transition (MST) with a large maximum reversible magnetic entropy change of ΔS_M =16.1 J kg^{-1} K^{-1} (this is about a four-fold increase compared to the ΔS_M observed for the bulk sample of the same nominal composition) and RC =144 J kg^{-1} for $\mu_o \Delta H$ = 5 T at temperature $T = T_M$ ~ 245 ± 1 K. The increase in the ΔS_M peak value leads to an improved RC compared to that of the bulk sample (122 J kg^{-1}). The observed MCE and quasi-

reversible character of ΔS_M at the MST illustrates the potential of $Ni_{0.895}Cr_{0.105}MnGe_{1.05}$ ribbons for magnetic cooling technology.

Keywords: Ni-Mn-Ge alloy ribbons; magnetocaloric effect; magnetostructural coupling; martensitic transformation.

[a]Author to whom correspondence should be addressed. Electronic mail: aryalanil@siu.edu (Anil Aryal)
[b]Author to whom correspondence should be addressed. Electronic mail: jose.sanchez@ipicyt.edu.mx (J.L. Sánchez Llamazares)

I. INTRODUCTION:

In recent years, materials undergoing first-order magnetostructural transformation (MSTs) have gained considerable scientific and technological interest since they exhibit a variety of interesting magnetoresponsive properties such as giant magnetocaloric effects (MCEs), magnetoresistance, magnetostriction, and magnetic shape memory effects [1-5]. The ternary stoichiometric compound NiMnGe undergoes two separate phase transitions that occur in well-separated temperature ranges [6]: (i) a magnetic phase transition of second-order from a spiral antiferromagnetic (AFM) phase to paramagnetic phase (PM) at a Neel temperature (T_N) of ~ 346 K, and (ii) a first-order structural martensitic transition from an orthorhombic TiNiSi-type structure (hereafter referred as martensite) to a hexagonal Ni_2In-type structure (hereafter referred as austenite) at a temperature (T_M) of ~ 470 K in the paramagnetic region. Successful attempts have been made to vary the transition temperatures to achieve a MST, that results in a change of the magnetic state of the material through a change in crystal structure, thereby affecting the abovementioned magnetoresponsive properties. Common methods employed to achieve coupled MSTs in these compounds are to change the stoichiometry [7, 8], introduce transition metal vacancies [9, 10], dope with extra elements [11-17], apply physical pressure [18], and isostructural alloying [19].

In NiMnGe based compounds, two types of MSTs have been reported. A MST from AFM martensite to ferromagnetic (FM) austenite obtained by decreasing the martensitic transition

temperature (T_M) below the Curie temperature of the austenite (T_C^A ~ 205 K) [7-9, 11, 12, 14, 17], and another type (field-induced MST) obtained by decreasing T_M and stabilizing it in the temperature window between T_N ~ 346 K and T_C^A ~ 205 K [15, 19, 20]. In the latter type, a magnetic field induces an AFM-FM transition in the martensitic state and a MST from a FM martensite to a PM austenite state is observed. The origin of the AFM-FM transition is attributed to the instability of the AFM magnetic structure of the martensite as demonstrated in previous studies [6, 14, 16].

In NiMnGe-based alloys, large magnetocaloric effects in terms of the maximum entropy change $|\Delta S_M^{peak}|$ associated with a coupled magnetostructural transition have been reported in $Ni_{1-x}Co_xMnGe_{1.05}$ [8], $Mn_{1.9-x}Ni_xGe$ [9], $MnNiGe_{1-x}Al_x$ [11, 12], $NiMn_{0.89}Cr_{0.11}Ge$ [13], and $Mn_{1-x}Fe_xNiGe$ [21] bulk alloys. However, as is typical of any first-order MST, such large MCE values are obtained in narrow temperature ranges with significant hysteresis loss due to irreversibility [22, 23]. Hence, a large reversible ΔS_M at a first-order MST can make a great impact on the usefulness of the MCE in this system.

The synthesis of magnetocaloric materials by rapid quenching using melt-spinning techniques has gained significant attention in the last years because of the following advantages: (a) it is a single step process to obtain homogeneous, single phase, and highly textured alloys with improved magnetocaloric properties; (b) annealing times and temperatures can be shortened or reduced significantly; and (c) is a continuous and mass production technique to produce any material of technological or industrial interest [24].

The magnetic and magnetcaloric properties of off-stoichiometric $NiMnGe_{1.05}$ have been investigated in bulk and ribbon forms [8, 25]. In ref. [7], the partial substitution of Cr in the Ni site in off-stoichiometric bulk $NiMnGe_{1.05}$ has been studied. A first-order MST from an orthorhombic AFM state to a hexagonal non-collinear FM state was reported in bulk $Ni_{1-x}Cr_xMnGe_{1.05}$ alloys for the compound with x = 0.105, which exhibits both direct and inverse MCEs with ΔS_M^{peak} = - 4.5 J kg^{-1} K^{-1} and 4.0 J kg^{-1} K^{-1} near T_C and T_M, respectively for

$\mu_o \Delta H$ = 5 T. Taking into account the advantages in getting highly homogeneous alloys using melt spinning technique, in this work we synthesized Cr doped $Ni_{0.895}Cr_{0.105}MnGe_{1.05}$ ribbons, and studied its crystal structure, and magnetic and magnetocaloric properties.

II. EXPERIMENTAL TECHNIQUES:

A bulk polycrystalline sample of nominal composition $Ni_{0.895}Cr_{0.105}MnGe_{1.05}$ was prepared using conventional arc-melting techniques under a controlled highly pure Argon atmosphere, as described in Ref. [7]. From this arc-melted ingot, melt-spun ribbon flakes of nominal composition ($Ni_{0.895}Cr_{0.105}MnGe_{1.05}$) were fabricated using an Edmund Bühler model SC melt spinner system under a highly pure Argon atmosphere with a linear speed of the rotating copper wheel of 25 ms^{-1}. Some of the ribbons were placed in a tantalum (Ta) envelope and thermally annealed at 1123 K (850 ^oC) for 48 h followed by water quenching. Both as-quenched and annealed ribbons were studied by different characterization techniques as described hereafter.

A high resolution Rigaku Smartlab diffractometer (CuKα radiation) was used to study the room temperature phase constitutions and crystal structures of the ribbon samples. The patterns were measured both on powdered and ribbon flakes separately. The microstructures of the ribbons were studied using a dual beam Helios Nanolab, ESEM FEI Quanta 200 scanning electron microscope (SEM). Differential scanning calorimetry (DSC) measurements were performed using a DSC 8000 instrument (with a ramp rate of 30 K/min during heating and cooling) in the temperature range 123 - 423 K. The latent heat (L) was estimated from the endothermic peaks of the heat flow curves using $L = \int_{T_s}^{T_f} \frac{\Delta Q}{\Delta T} dT$, where $\frac{\Delta Q}{\Delta T}$ is the change in heat flow with respect to temperature, and T_s and T_f are the initial and final temperatures of the magnetostructural phase transitions on heating, respectively.

Magnetization measurements were performed at DC-magnetic fields ($\mu_o H$) using a 9 T Quantum Design PPMS® Dynacool® platform and the vibrating sample magnetometry (VSM) option. The magnetic and magnetoloric properties were measured on a needle-like ribbon sample applying the magnetic field along the long axis in order to minimize the internal demagnetizing field. The thermal dependence of the magnetization, i.e., the *M(T)* curves, were measured from 10 to 400 K with a heating / cooling rate of 1.5 K / min at low and high magnetic fields of 5 mT and 5 T, respectively. The samples were first cooled to 10 K from 400 K at zero field. The zero-field-cooling (ZFC) measurements were taken while heating the samples to 400 K in an applied magnetic field, and then followed by field-cooling (FC) measurement to 10 K and field-heating (FH) measurement from 10 K to 400 K. The phase transition temperatures were determined from the minimum of the dM/dT vs. T curves in *M(T)* during the heating cycle. In the case of first-order magnetostructural transition (i.e., for the annealed ribbons), a set of isothermal magnetization curves $M(\mu_o H)$ were measured through the first-order transition on heating from 200 to 259 K up to a maximum applied magnetic field of 5 T. The thermal protocol used to measure each of these curves was as follows: with the magnetic field set to zero, the sample was first heated to 300 K, cooled to 100 K, and heated again to the measuring temperature. After temperature stabilization the isothermal magnetization curve was measured. This thermal protocol avoids an over estimation of the $|\Delta S_M^{peak}|$ value and ensures a correct T location for the maximum of the $\Delta S_M(T)$ curve [26].

III. RESULTS AND DISCUSSIONS:

Typical SEM images of the microstructure of as-quenched and annealed melt-spun ribbons are shown in Figure 1 (a) and (b), respectively, whereas the typical fractured cross-section of as-quenched ribbons with an average thickness 15 ± 1 μm is shown at the inset of Fig. 1(a). The free surface of as-quenched ribbons (see Fig. 1(a)) showed a polyhedron

granular microstructure with some porosity. On the fractured cross-section of (see inset of Fig. 1(a)), a fully crystalline microstructure of columnar in shape grains whose longer axis tends to orient perpendicular to both ribbon surfaces were observed. Such a columnar-like microstructure indicates the presence of a preferred texture of these ribbons. As shown in Figure 1(b), the average grain size of ribbons considerably increases upon thermal annealing with well-defined grain boundaries. Furthermore, inside some grains that belong to the hexagonal phase, some straight lines appear indicating the presence of ferroelastic domain walls (FEDW), as observed in the isostructural MnCoGe-based alloys [27]. The improvement of the homogeneity of the grain distribution was also observed after thermal treatment (see in Fig. 1(b)).

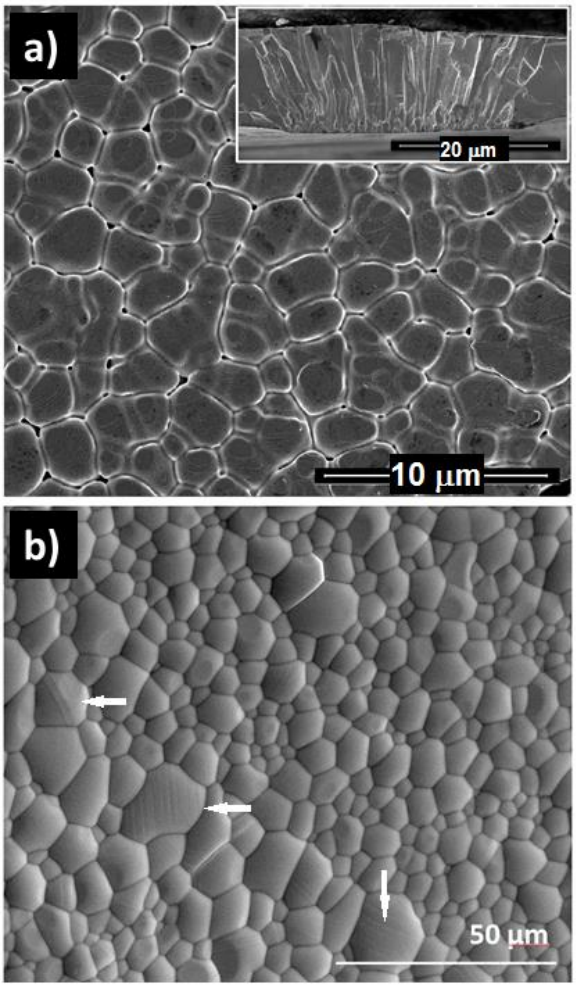

Figure 1. Typical SEM micrograph of free surface microstructure of (a) as-solidified and (b) annealed $Ni_{0.895}Cr_{0.105}MnGe_{1.05}$ melt-spun ribbons. Inset: typical cross-sectional micrograph of fractured as-solidified melt-spun ribbons that show an average thickness of 15 ± 1 μm. Arrows in (b) indicate the ferro-elastic domains in the grains.

Room temperature XRD patterns of $Ni_{0.895}Cr_{0.105}MnGe_{1.05}$ ribbons measured on both powdered and flat flake ribbons are shown in Figure 2 (a)-(c). A single-phase hexagonal Ni_2In-type structure characterized by cell parameters a = 4.086(1) Å and c = 5.392(1) Å at room temperature was observed for the ribbons. Thus, the melt spinning technique is an effective single-step process to obtain a single-phase compound directly from the melt as previously reported for MnCoGe-based alloys [27, 28]. The crystal structure and the cell parameters are consistent with those previously reported for the counterpart bulk alloys [7]. The XRD patterns obtained from the surface of flat flakes show a relative increase in the intensity of the (002) and (004) peaks, conforming the ribbons texture along the (*00l*) direction, which is consistent with the SEM images (see Figure 2 (b)).

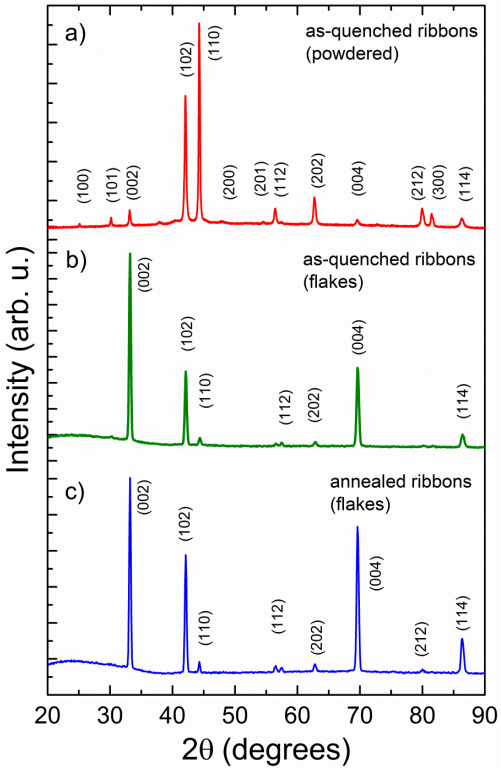

Figure 2. Room temperature X-ray diffraction patterns of $Ni_{0.895}Cr_{0.105}MnGe_{1.05}$ ribbons: (a) as-quenched powdered ribbons, (b) as-quenched ribbon flakes, and (c) annealed ribbon flakes. The XRD peak indexing was done based on the hexagonal Ni_2In-type crystal structure.

The temperature-dependent magnetization data, $M(T)$, of the as-quenched and annealed ribbons measured at magnetic fields of 5 mT and 5 T are shown in Figure 3 (a) and (b), respectively. The measurements were taken following the zero-field-cooled (ZFC), field-cooled (FC), and field-heating (FH) protocols. A second-order magnetic transition (SOT) from the FM to PM state was observed in the as-quenched ribbons at the Curie temperature of the hexagonal structure (T_C^A) ~ 192 ± 1 K and 210 ± 1 K at $\mu_0 H$ = 5 mT and 5 T, respectively. On the contrary, the phase transition for the annealed ribbons clearly shows a thermal hysteresis in the $M(T)$ curves at T_M = 245 ± 1 K during heating and cooling cycles, as shown in the inset of Fig. 3(b). The presence of thermal hysteresis indicates a temperature induced first order transition (FOT) from a high temperature austenite (hexagonal) to a low temperature martensite (orthorhombic) structure. Increasing the temperature, a sharp jump in magnetization was observed at a transition temperature (T_t) = 185 ± 1 K. Neutron diffraction studies in NiMnGe compounds by W. Bazela et. al. [6, 16] have shown that the magnetic state of NiMnGe compounds in their martensite phase (MP) at low temperatures undergo a reorientation of the spiral axis at T_t = 185 K. At temperatures $T < T_t$, the spiral axis lies in the *bc* plane, and for $T_t < T < T_N$ the spiral axis is parallel to the *a*-axis. Referring to the results of their study on neutron diffraction, this additional transition observed at T_t ~ 185 K is related to the reorientation of the spiral axis. The ribbons show sharp changes in magnetization with a further increase in temperature, which corresponds to magnetic transitions from the AFM to the PM state. Thus, a MST as a result of coupling of the structural (characterized by temperature hysteresis) and magnetic transitions at T_M = 245 ± 1 K was observed in the annealed ribbons at low applied magnetic field.

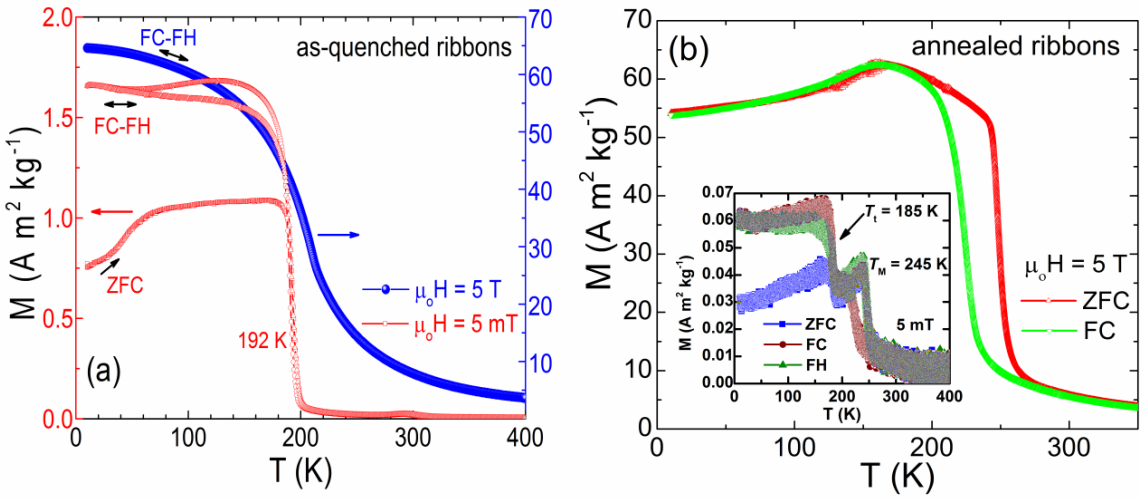

Figure 3. Temperature dependence of magnetization of $M(T)$ of (a) as-quenched and (b) annealed ribbons measured under static magnetic fields of $\mu_o H$ = 5 mT and 5 T. The ZFC, FC and FH protocols followed are indicated in the figure by black arrows. Inset of (b): $M(T)$ curves of annealed ribbons at $\mu_o H$ = 5 mT.

At $\mu_0 H$ = 5 T, a large difference between the magnetizations (ΔM = 44 A m^2 kg^{-1}) was observed at T_M as shown in Figure 3(b). Such a large change in magnetization indicates a field-induced transition between magnetic states (spiral AFM structure to parallel FM structure) of the martensite, followed by a FM-PM type MST. In order to study the transition at zero magnetic field, a DSC measurement was performed. As shown in Figure 4, well-defined endothermic / exothermic peaks with thermal hysteresis during heating / cooling cycles in the heat flow curves verify the first-order behavior of the MST. The values of the latent heat (L) and corresponding total entropy change (ΔS_T) obtained from DSC were found to be 8.3 kJ kg^{-1} and 33.0 J kg^{-1} K^{-1}, respectively. A small anomaly above T_M = 248 K on the heat flow curve during heating was observed which is related to the magnetic transition from the AFM / FM to the PM phase. A similar anomaly in the heat flow curves has been previously reported in NiMnGe systems in Refs [7, 11, 12].

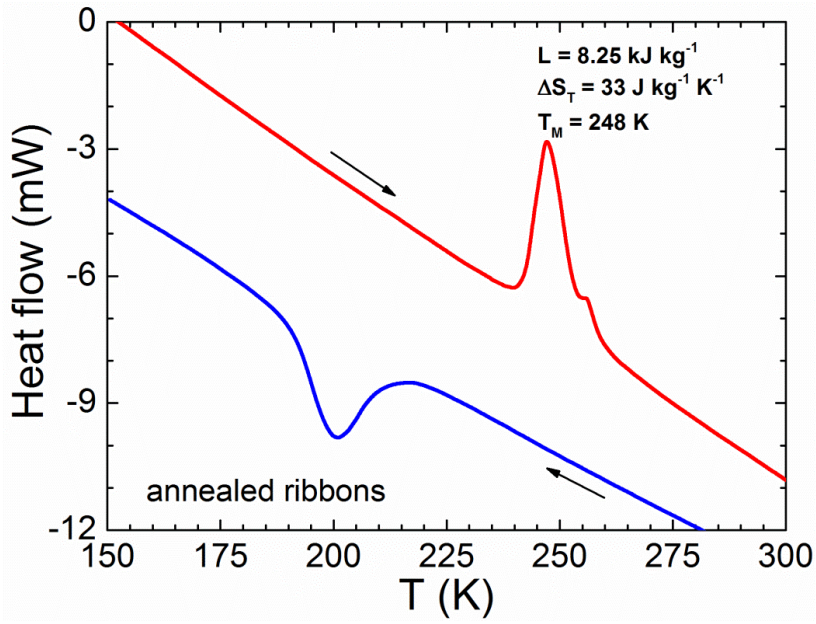

Figure 4. DSC heat flow curves of annealed melt-spun ribbons. Arrows indicate the direction of heating and cooling.

Figures 5 (a) and (b) show the isothermal magnetization $M(\mu_0 H)$ curves up to 5 Tesla measured in the vicinity of SOT and first-order MST temperatures for as-quenched and annealed ribbons, respectively. At temperatures $T < T_C^A$, the as-quenched ribbons show a FM behavior, whereas at $T > T_C^A$ a linear paramagnetic behavior in the $M(\mu_0 H)$ curves is observed. For annealed ribbons, a field-induced metamagnetic behavior is observed in the vicinity of T_M. In the low magnetic field region, the $M(\mu_0 H)$ curves tend to exhibit a quasi-linear behavior indicating an AFM type of magnetic state in the martensite. When the applied field increases, a jump-like change in slope at a critical field ($\mu_0 H_{CR}$) in the $M(\mu_0 H)$ curve reveals a field-induced metamagnetic transition from a spiral AFM structure (as concluded from a neutron diffraction study published in Ref. [6]) to a canted FM state. Further increasing the magnetic field to the saturation field ($\mu_o H_S$), the canted FM state transform to a collinear FM state and saturates. Thus, in annealed ribbons a field-induced AFM-FM transition of the martensite phase appears in the vicinity of T_M. Such a sequence of transitions can be described as a field-induced transition from an AFM to FM martensitic phase, and then

a temperature-induced transition to paramagnetic austenitic phase with a large ΔM, similar to that reported in Ref. [20, 21].

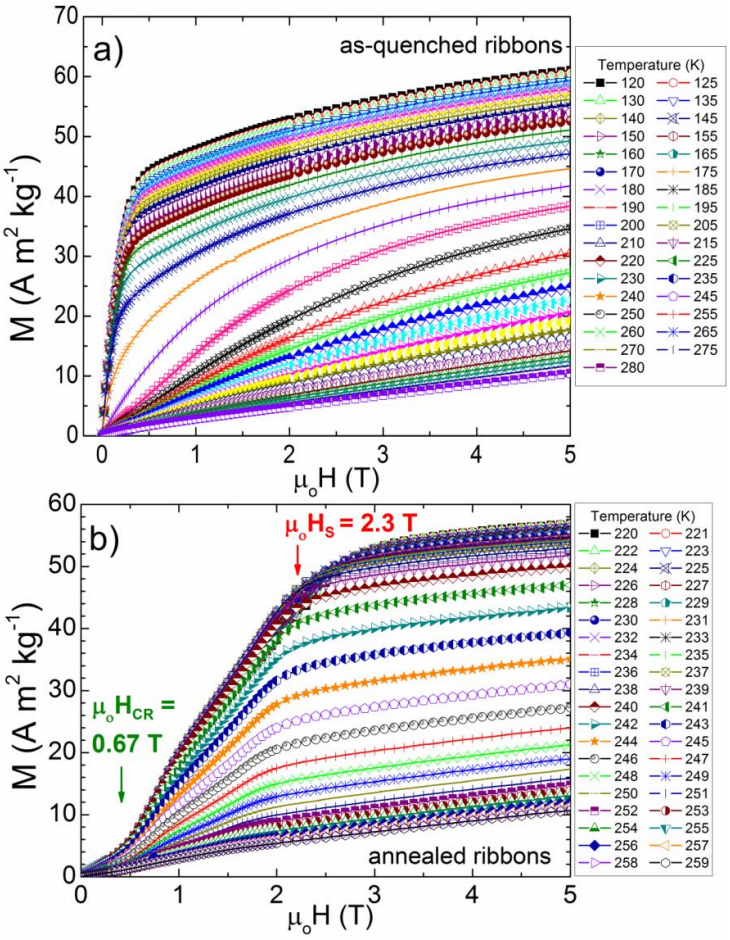

Figure 5. Isothermal magnetization curves of (a) as-quenched and (b) annealed ribbons measured up to a maximum magnetic field of $\mu_o H$ = 5 T.

From the isothermal $M(\mu_0 H)$ curves, $dM/d(\mu_0 H)$ vs $\mu_0 H$ curves, and hence a $\mu_0 H$-T phase diagram, were plotted for annealed ribbons (Figure 6). As can be seen in the $dM/d(\mu_0 H)$ curves (inset of Fig. 6), three prominent inflection points, referred as I_1, I_2, and I_3 exist. The magnetic field value corresponding to peak I_1 defines the critical field ($\mu_0 H_{CR}$) at which the metamagnetic transition from the AFM to the canted FM state starts. The second peak (I_2) suggests a complex process of the field-induced transition of the magnetic phase of the martensite from a canted FM state to a collinear FM phase. Finally, the peak I_3 represents the

saturation of the collinear FM state of the martensite at the saturation field, $\mu_0 H_S$. The aforementioned evolution of the magnetic phase of the martensite with applied magnetic field and temperature is further shown in the magnetic phase diagram (see Fig. 6). For a magnetic field $\mu_0 H < \mu_0 H_{CR}$, the martensite is in a spiral AFM state. With increasing field and $\mu_0 H_{CR} \leq \mu_0 H < \mu_0 H_S$, a competition and transition of the AFM state to a canted FM state is established. For $\mu_0 H > \mu_0 H_S$, the field-induced transition of the magnetic state of the martensite is complete, and saturation of the FM state occurs. With increasing temperature, $\mu_0 H_{CR}$ remains almost unchanged, whereas $\mu_0 H_S$ decreases significantly. Further increase in temperature results in the MST from a FM TiNiSi-type to a PM Ni_2In-type phase.

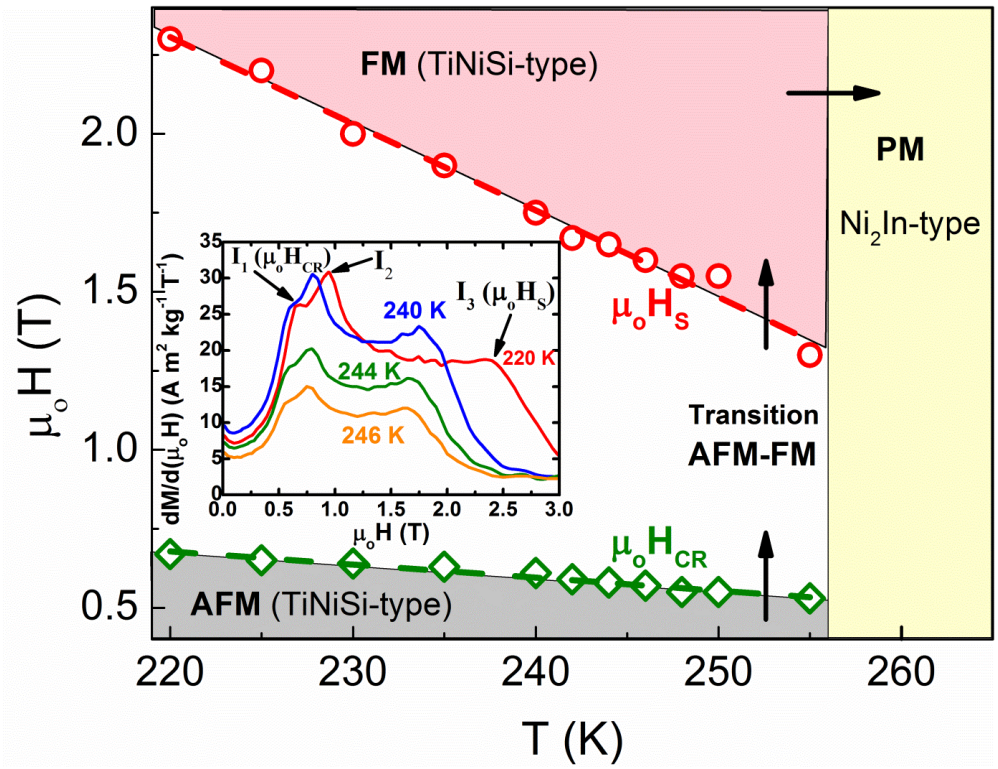

Figure 6. Magnetic phase diagram constructed from the derivative of the $M(\mu_o H)$ curves for annealed ribbons. Inset: $dM/d(\mu_o H)$ vs $\mu_o H$ curves at selected temperatures.

Additionally, it is interesting to note that the set of magnetization isotherms measured with increasing and decreasing magnetic field across the phase transition temperature in both

ribbons showed zero hysteresis loss, indicating a completely reversible process (see the inset of Fig. 7 (a) and (b)). Such a magnetic reversibility is of great importance in first-order MST and SOT materials to maximize the ΔS_M and hence the MCE [29, 30].

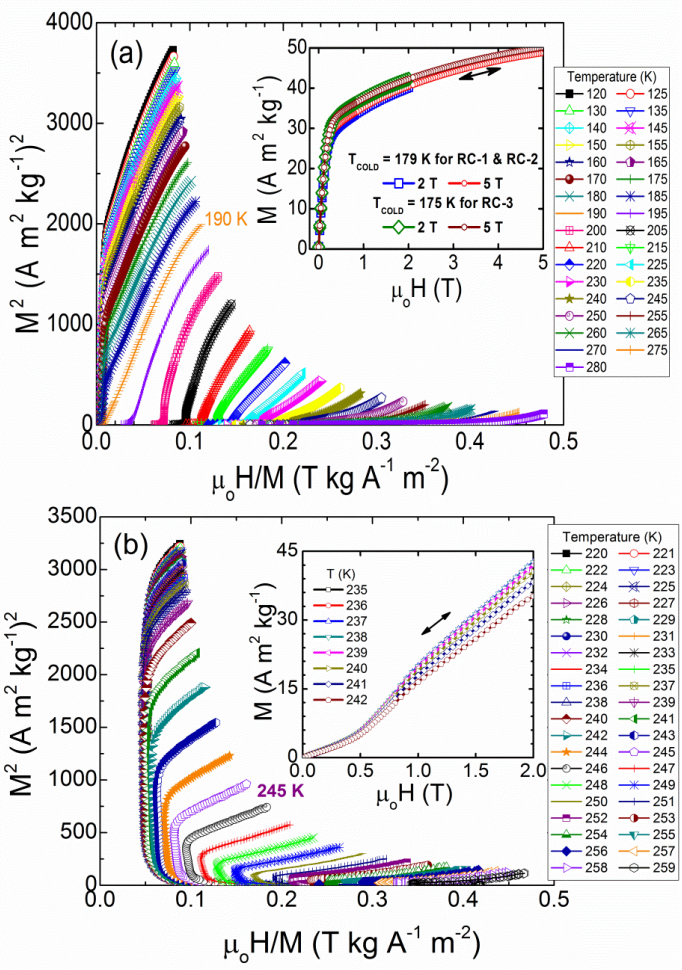

Figure 7. The Belov-Arrott plots of M^2 vs $\mu_o H/M$ of (a) as-quenched and (b) annealed $Ni_{0.895}Cr_{0.105}MnGe_{1.05}$ melt-spun ribbons. Inset of (a): reversibility of isothermal magnetization curves for as-quenched ribbons measured at 179 K and 175 K sweeping magnetic field up and down (shown by the double arrows) to maximum values of 2 T and 5 T. These temperatures correspond to T_{cold} for δT_{FWHM} (for *RC*-1 and *RC*-2) and δT (for *RC*-3) Inset of (b): reversibility of magnetization isotherms on increasing and decreasing magnetic field up to $\mu_o H$ = 2 T for the annealed ribbons across the phase transition temperatures and around its determined cold sink.

In order to verify the nature of the phase transition, Belov-Arrott plots, i.e, M^2 as a function of $\mu_0 H/M$ [31], were plotted. As shown in Figure 7 (a), a positive slope of the curves confirms the second-order nature of the FM-PM transition in the as-quenched ribbons [32]. From the Belov-Arrott plot, the Curie temperature (T_C^A) was found to be 190 K. T_C^A was defined as the temperature at which the curvature of $\mu_0 H$ vs M^2 curve changes sign and passes through origin. Notice that the values of T_C^A obtained from Belov-Arrott plot (~ 190 K) and from $M(T)$ measurement from minimum dM/dT (192 K) are in good agreement. On the contrary, Belov-Arrott plots for the annealed ribbons showed the typical S-shaped curves with negative slope near T_M as seen in Fig. 7 (b), which suggests the first-order phase transition [32].

Figure 8 shows the temperature dependence of the magnetic entropy changes, $\Delta S_M(T)$, in the vicinity of the SOT (for as-quenched ribbons) and the MST (for annealed ribbons) for a magnetic field change of $\mu_0 \Delta H = 5$ T. The ΔS_M curves at several field changes were calculated using the integrated Maxwell relation $\Delta S_M(T, \mu_o \Delta H) = \mu_o \int_0^{\mu_o H_{max}} \left[\frac{\partial M(T,\mu_o H')}{\partial T}\right]_{\mu_o H'} dH'$ from the magnetization isotherms measured at different temperatures (shown in Figure 5). A direct MCE (with negative ΔS_M) has been observed in both as-quenched and annealed ribbons as shown in Figures 8(a) and (b). The peak value of $\Delta S_M^{peak} = 4.4$ J kg^{-1} K^{-1} at 5 T was found for as-quenched ribbons, which is associated with a second order FM-PM transition. A much larger ΔS_M^{peak} value of 16.1 J kg^{-1} K^{-1} at $\mu_0 \Delta H = 5$ T was found in the annealed sample. Such a large value of ΔS_M is due to the magnetic-field induced first-order MST observed in the annealed ribbons. The obtained values of ΔS_M^{peak} in the annealed ribbons is a more than four-fold increase compared to those reported for bulk $Ni_{1-x}Cr_xMnGe_{1.05}$ with x = 0.105 (i.e, ΔS_M^{peak} of 4.0 J kg^{-1} K^{-1} at T_M and - 4.5 J kg^{-1} K^{-1} at T_C), and more than double that reported for $NiMnGe_{1.05}$ melt-spun ribbons (5.8 J kg^{-1} K^{-1} at T_M) at $\mu_0 H = 5$ T [7, 25].

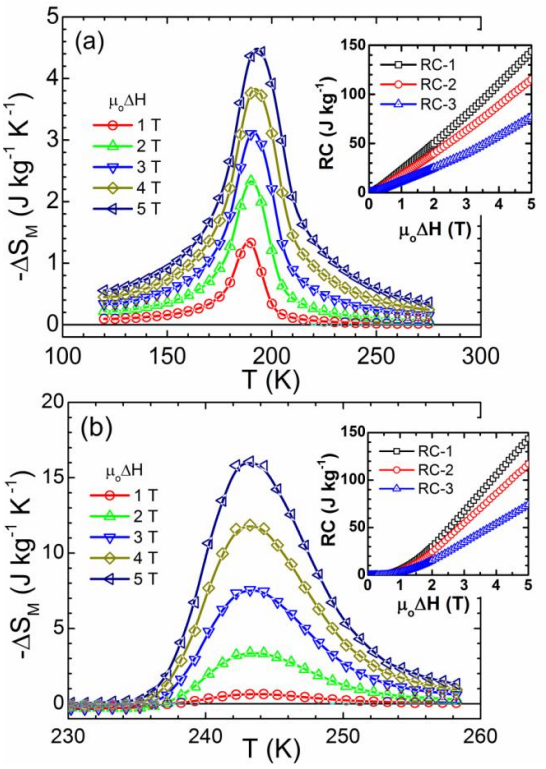

Figure 8. Magnetic entropy change ΔS_M as a function of temperature for different magnetic field changes for $Ni_{0.895}Cr_{0.105}MnGe_{1.05}$ (a) as-solidified, and (b) annealed melt-spun ribbons. Insets: Field dependence of refrigerant capacities *RC*-1, *RC*-2, and *RC*-3.

The refrigeration capacity (*RC*) is an important parameter that estimates the usefulness of a material as a coolant for magnetic refrigeration. It measures the amount of heat that can be transferred between the hot and cold reservoirs in an ideal refrigeration cycle. The *RC* has been estimated by the following three methods: (a) the product $|(\Delta S_M)_{peak}| \times \delta T_{FWHM}$ (referred to as *RC*-1), where $\delta T_{FWHM} = T_{hot} - T_{cold}$ are the temperatures that define the full-width at half-maximum of $\Delta S_M(T)$; (b) the area under the $\Delta S_M(T)$ curve between T_{hot} and T_{cold} (referred to as *RC*-2); and (c) the maximum of the product $\Delta S_M \times \delta T$ below the $\Delta S_M(T)$ curve (referred to as *RC*-3; i.e., the Wood and Potter criterion) [33 and refs. therein]. Large RC values of 144 J kg^{-1} (*RC*-1), 117 J kg^{-1} (*RC*-2), and 74 J kg^{-1} (*RC*-3) were found for annealed ribbons at 5 T. The *RC*-1 value is greater than those reported for its bulk counterpart (~ 65 J kg^{-1} at T_M and ~122 J

kg^{-1} near T_C, estimated from the $\Delta S_M(T)$ curves reported in Ref. [7]). The magnetic field change dependences of *RC*-1, *RC*-2, and *RC*-3 for as-quenched and annealed ribbons are shown in the inset of Figures 8 (a) and (b), respectively. The summary of magnetocaloric properties of $Ni_{0.895}Cr_{0.105}MnGe_{1.05}$ ribbons (as-quenched and annealed) is given in Table 1.

$Ni_{0.895}Cr_{0.105}MnGe_{1.05}$ melt-spun ribbons as-solidified / annealed (850 ^oC during 48 h)					
$\mu_o\Delta H$ (T)	**1.0**	**2.0**	**3.0**	**4.0**	**5.0**
$\lvert\Delta S_M^{peak}\rvert$ (J kg^{-1} K^{-1})	1.3 / 0.6	2.3 / 3.4	3.1 / 7.6	3.8 / 11.9	4.4 / 16.1
***RC*-1 (J kg^{-1})**	23 / 6	50 / 30	79 / 67	111 / 105	144 / 144
***RC*-2 (J kg^{-1})**	18 / 5	40 / 24	63 / 55	89 / 86	115 / 117
δT_{FWHM} (K)	17 / 9	21 / 9	26 / 8	30 / 9	32 / 9
T_{hot} (K)	197 / 249	200 / 249	204 / 248	207 / 248	209 / 248
T_{cold} (K)	180 / 240	179 / 240	178 /240	177 / 239	177 / 239
***RC*-3 (J kg^{-1})**	11 / 3	25 / 15	39 / 35	58 / 54	77 / 74
δT^{RC-3} (K)	15 / 8	21 / 7	29 / 7	65 / 7	72 / 7
T_{hot}^{RC-3} (K)*	196 / 248	200 / 247	205 / 247	222 / 247	228 / 247
T_{cold}^{RC-3} (K)*	181 / 240	179 / 240	176 / 240	157 / 240	156 / 240

***related to *RC*-3.**

Table 1. Magnetocaloric effects and related parameters in $Ni_{0.895}Cr_{0.105}MnGe_{1.05}$ melt-spun ribbons.

IV. CONCLUSIONS:

In conclusion, rapidly solidified polycrystalline $Ni_{0.895}Cr_{0.105}MnGe_{1.05}$ ribbons were synthesized using a melt-spinning technique, and their crystal structures and magnetocaloric properties were studied in as-quenched and annealed states. A single-phase hexagonal Ni_2In-type crystal structure was observed at room temperature for both ribbons. The as-quenched ribbons showed a second order magnetic transition with ΔS_M^{peak} = 4.4 J kg^{-1} K^{-1} with $\mu_o\Delta H$ = 5 T. A magnetic field-induced transition from an AFM to a FM state in the martensite structure was observed in annealed ribbons, which led to a coupled MST from a FM martensite to a PM austenite state with a large change in magnetization. As a result of the field-induced MST, a large ΔS_M^{peak} value of 16.1 J kg^{-1} K^{-1} (which is about a four times larger than the bulk) and *RC*-1 =144 J kg^{-1} at $\mu_0\Delta H$ = 5 T was found. Both ribbon samples showed excellent magnetic reversibility. The large value and reversible character of ΔS_M at the first-

order MST illustrates the potential for $Ni_{0.895}Cr_{0.105}MnGe_{1.05}$ ribbons fabricated using melt-spinning technique to be applied in magnetic cooling technology.

Acknowledgements: This work was supported by the U.S. Department of Energy (DOE), Office of Science, Basic Energy Sciences (BES) under Award No. DE-FG02-06ER46291 (SIU) and DE-FG02-13ER46946 (LSU). The authors acknowledge financial support received from Laboratorio Nacional de Investigaciones en Nanociencias y Nanotecnología (LINAN, IPICyT). C.F. Sánchez-Valdés is grateful to DMCU-UACJ for supporting his 2017 summer research stay at IPICyT (program PFCE and academic mobility grant); also, for the financial support received from CONACYT (Grant No. 286993) and PRODEP-SEP (Grant No. UACJ-PTC-383), Mexico. The technical support of M.Sc. B.A. Rivera-Escoto and M.Sc. A.I. Pérez-Maldonado (from LINAN) is gratefully acknowledged.

References:

[1] A. O. Pecharsky, K. A. Gschneidner, Jr, and V. K. Pecharsky, J. Appl. Phys. 93, 4722 (2003).

[2] O. Tegus, E. Bruck, K. H. J. Buschow, and F. R. de Boer, Nature (London) 415, 150 (2002).

[3] T. Krenke, E. Duman, M. Acet, E. F. Wassermann, X. Moya, L. Mañosa, and A. Planes, Nat. Mater. 4, 450 (2005).

[4] S. Y. Yu, Z. H. Liu, G. D. Liu, J. L. Chen, Z. X. Cao, G. H. Wu, B. Zhang, and X. X. Zhang, Appl. Phys. Lett. 89, 162503 (2006).

[5] R. Kainuma, Y. Imano, W. Ito, Y. Sutou, H. Morito, S. Okamoto, O. Kitakami, K. Oikawa, A. Fujita, T. Kanomata, and K. Ishida, Nature (London) 439, 957 (2006).

[6] W. Bazela, A. Szytuła, J. Todorovic´, Z. Tomkowicz, and A. Zieba, Phys. Status Solidi A 38, 721 (1976)

[7] A. Aryal, A. Quetz, S. Pandey, M. Eubank, T. Samanta, I. Dubenko, S. Stadler, and N. Ali, J. Appl. Phys. 117, 17A711 (2015)

[8] C. Zhang, D. Wang, Q. Cao, S. Ma, H. Xuan, and Y. Du, J. Phys. D: Appl. Phys. 43, 205003 (2010).

[9] C. L. Zhang, D. H.Wang, Q. Q. Cao, Z. D. Han, H. C. Xuan, and Y. W. Du, Appl. Phys. Lett. 93, 122505 (2008).

[10] C. L. Zhang, C. Zhu, J. Chen, T. Z. Wang, Z. D. Han, J. Appl. Phys. 112, 123911 (2012).

[11] A. Quetz, T. Samanta, I. Dubenko, M.J. Kangas, J.Y. Chan, S. Stadler, N. Ali, J. Appl. Phys. 114 153909 (2013)

[12] T. Samanta, I. Dubenko, A. Quetz, S. Temple, S. Stadler, and N. Ali, Appl. Phys. Lett. 100, 052404 (2012)

[13] A.P. Sivachenko, V.I. Mityuk, V.I. Kaomenev, A.V. Golovchan, V.I. Valkov, I. F. Gribanow, Low Temp. Phys. **39** 1051 (2013)

[14] E. Liu, Y. Du, J. Chen, W. Wang, H. Zhang and G. Wu, IEEE Trans. Magn., **47**, 4041-4043 (2011)

[15] E. K. Liu, W. H. Wang, L. Feng, W. Zhu, G. J. Li, J. L. Chen, H. W. Zhang, G. H. Wu, C. B. Jiang, H. B. Xu, and F. R. de Boer, Nat. Commun. **3**, 873 (2012).

[16] W. Bazela, A. Szytuła, J. Todorovic´, and A. Zieba, Phys. Status Solidi A 64, 367 (1981)

[17] C. L. Zhang,Z. D. Han,B. Qian,H. F. Shi,C. Zhu,J. Chen, T. Z. Wang, J. Appl. Phys.**114**, 153907 (2013)

[18] S. Anzai and K. Ozawa, Phys. Rev. B **18**, 2173 (1978).

[19] E. K. Liu, H. G. Zhang, G. Z. Xu, X. M. Zhang, R. S. Ma, W. H. Wang, J. L. Chen, H. W. Zhang, G. H. Wu, L. Feng, and X. X. Zhang, Appl. Phys. Lett. **102**, 122405 (2013)

[20] S. C. Ma, D. Hou, F. Yang, Y. L. Huang, G. Song, Z. C. Zhong, , D. H. Wang, Y. W. Du, Appl. Phys. Lett. **104**, 202412 (2014)

[21] K. Xu, Z. Li, E. Liu, H. Zhou, Y. Zhang, C. Jing, Sci. Rep. 7, 41675 (2017)

[22] V. Provenzano, A. J. Shapiro and R. D. Shull, Nature **429**, 853 (2004)

[23] Y. Koshkid'ko, S. Pandey, A. Quetz, A. Aryal, I. Dubenko, J. Cwik, E. Dilmieva, A. Granovsky, E. Lähderanta, S. Stadler, N. Ali, J. Magn. Magn. Matter, (2017) https://doi.org/10.1016/j.jmmm.2017.11.125

[24] B. Hernando, J. L. Sánchez Llamazares, J. D. Santos, V. M. Prida, D. Baldomir, D. Serantes, R. Varga, and J. González, , Appl. Phys. Lett. **92**, 132507 (2008)

[25] Gerardo Daniel-Perez, J. L. Sanchez Llamazares, A. Quintana-Nedelcos, P. Alvarez-Alonso, R. Varga, V. Chernenko, J. Appl. Phys. 115, 17A920 (2014)

[26] A. Quintana-Nedelcos, J. L. Sánchez-Llamazares, C. F. Sánchez-Valdés, P. Álvarez Alonso, P. Gorria, P. Shamba, N. A. Morley, J. Alloys Compd. **694**, 1189 (2017)

[27] A. Quintana-Nedelcos, J. L. Sánchez Llamazares, H. Flores-Zúñiga, J. Alloys Compd., **644** 1003 (2015)

[28] C.F. Sánchez-Valdés, J. L. Sánchez Llamazares, H. Flores-Zúñiga, D. Rios-Jara, P. Alvarez, P. Gorria, Scripta Mater., **69** Issue 3 211 (2013)

[29] J. Ćwik, Y. Koshkidko, I. Tereshina, N. Kolchugina, K. Nenkov, A. Hackemer, J. Lyubina, T. Palewski, G.S. Burkhanov, M. Miller, J. Alloys Compd. **649**, 417 (2015)

[30] J. Ćwik, Y. Koshkid'ko, A. Mikhailova, N. Kolchugina, K. Nenkov, A. Hackamer, M. Miller, J. Appl. Phys. **117**, 123912 (2015)

[31] A. Arrott, Phys. Rev. **108** 1394 (1957)

[32] S. K. Banerjee, Phys. Lett. **12**, 16 (1964)

[33] J. L. Sánchez Llamazares, H. Flores-Zuñiga, C. Sánchez-Valdes, C. A. Ross, and C. García, J. Appl. Phys. **111**, 07A932 (2012)